A R C H I V E S O F M E T A L L U R G Y A N D M A T E R I A L S
Volume 52 2007 Issue 2

M. S. SZCZERBA*, T. TOKARSKI *, M. PEREK*

< 100 > BURGERS VECTOR DISLOCATIONS INHERITED BY SECOND OVERSHOOT FCC TWINNING

DYSLOKACJE O WEKTORZE BURGERSA TYPU < 100 > POWSTAŁE PODCZAS MECHANICZNEGO BLIŹNIAKOWANIA W MONOKRYSZTAŁACH RSC

TEM observations of <100> Burgers vector dislocations in twinned copper-aluminum alloy single crystals are reported. It is found that network of cube dislocations result from a growing twin and conjugate slip interactions which originate at the end of the second overshoot of the tensile deformation of low stacking fault energy FCC crystals. It is also found that the dislocation network of the cube dislocations is usually accompanied with another network of extrinsic Frank dislocations resulting from a dissociation of cube dislocation segments attached to the twin shear plane. The experimental results obtained in this paper fully support those reported in the paper by Basinski *et al.* [1], which showed that the cube dislocations may also result from a growing twin and primary slip interactions associated with the first overshoot FCC twinning.

Keywords: twin transformation, dislocations, FCC crystals

W pracy przedstawione są obserwacje elektronomikroskopowe dyslokacji o wektorze Burgersa <100> w monokryształach miedź-aluminium, które uległy bliźniakowaniu. Pokazano, że sieć dyslokacji kubicznych powstaje w skutek interakcji między powstającym bliźniakiem a dyslokacjami poślizgu sprzężonego, która rozpoczyna się z końcem II *overshootu* podczas rozciągania kryształów RSC o niskiej energii błędu ułożenia. Wykazano również, że sieci dyslokacji kubicznych zwykle towarzyszy sieć dyslokacji Franka stowarzyszonych z zewnętrznymi błędami ułożenia, które powstają z dysocjacji segmentów dyslokacji kubicznych przytwierdzonych do płaszczyzny ścięcia bliźniaczego. Wyniki eksperymentalne otrzymane w pracy potwierdzają te przedstawione w pracy Basinskiego i in. [1], w której pokazano, że dyslokacje kubiczne mogą również powstawać w wyniku interakcji między powstającym bliźniakiem a dyslokacjami poślizgu pierwotnego towarzyszącej zjawisku I *overshootowi* podczas bliźniakowania w kryształach o sieci RSC.

1. Introduction

B a s i n s k i and co-workers [1] have shown that twinned Cu-8at.%Al single crystals may contain a large number of *a* <100> Burgers vector dislocations resulting from interactions between a growing twin and pre-existing primary slip dislocation substructure, and the dislocation transformation is predictable by the correspondence matrix method [2]. They also found that the twinned crystal regions exhibit significantly larger strength than the twin-free matrix. B a s i n s k i and co-workers considered the case of mechanical twinning which originates in the course of the tensile deformation of FCC single crystals when the tensile axis initially located well in the center of the basic stereographic triangle overshoots by a few degrees the [001] – [$\bar{1}$11] symmetry line (Fig. 1a). Usually at this position in low-stacking-fault-energy FCC metals and alloys a changeover from primary slip dominance into deformation twinning operating on conjugate plane takes place [3].

The entry of twinning is then accompanied by a sudden drop of the tensile load which is associated with the nucleation of the first twin band. Further crystal deformation proceeds by nucleation of successive twin bands along the sample length and characteristic jerky flow is easily detectable on the tensile stress-strain curve. However, when the initial tensile orientation is located significantly closer to the [001]–[$\bar{1}$11] symmetry line (Fig. 1b) the overshoot position is achieved at much lower tensile strains, the critical stress conditions for deformation twinning are not met, and further crystal deformation proceeds by conjugate slip dominance instead [3]. This turns crystal tensile axis back to the basic stereograph-

* DEPARTMENT OF STRUCTURE AND MECHANICS OF SOLIDS, AGH UNIVERSITY OF SCIENCE AND TECHNOLOGY, 30-059 KRAKÓW, AL. MICKIEWICZA 30, POLAND

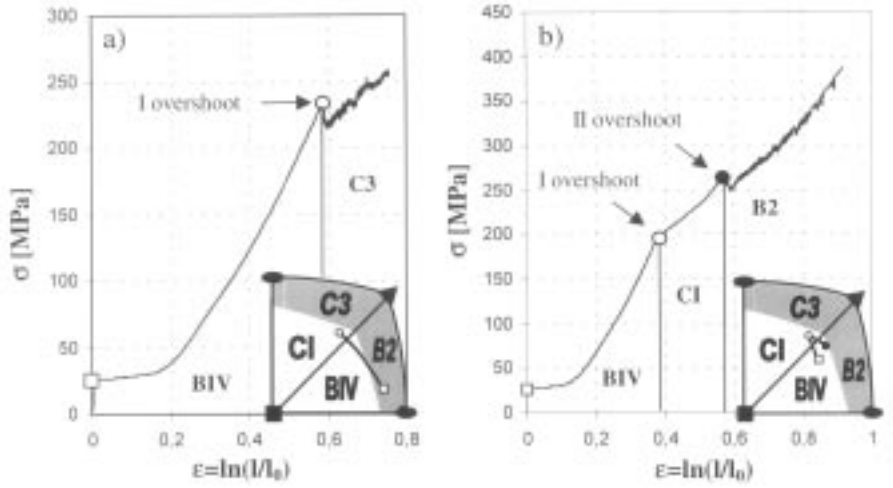

Fig. 1. Room temperature tensile characteristics of Cu-8at.%Al single crystals oriented for single (a), and nearly double slip (b). Note the inserts showing schematically rotation of the tensile axis before the entry of the I and the II overshoot twinning respectively. Note also that two stereographic triangles are divided into four regions named by suitable slip and twin systems according to the highest Schmid factor (the crystallography of B2, BIV, C3 and CI see further [4])

ic triangle and after crossing the symmetry line again the phenomenon of the second overshoot is observed (Fig. 1b). During the conjugate slip dominance the rate of work hardening is still profound and at the end of the second overshoot flow stress becomes high enough to satisfy the condition for deformation twinning to occur [4]. Now, twinning operates on the plane of the former primary slip, and in this case, what will be shown later, the origin of cube dislocations must differ from that of the first overshoot twinning.

The main aim of the present paper is firstly, to bring an experimental prove to the presence of the cube dislocations inherited by the second overshoot FCC twinning, secondly, to emphasize again the validity of the correspondence matrix method considered in the pioneer work of S l e e s w y k and V e r b r a a k [5] as a proper tool for geometrical description of the twin transformation of cube lattice defects. It is also germane to note, that although in the recent literature there is a number of papers [6-11] referring to the problem considered in this paper, they do not still contain any direct experimental evidences supporting the validity of the correspondence matrix method, except the report by C h i u et al. [12] on TEM observations of the twin transformation of faulted dipoles in a FCC-based lattice γ-TiAl compound.

2. Experimental procedure

The investigations were carried out on Cu-8at.%Al single crystals having the geometry of a rectangular prism 150×6×6 mm^3 and the initial orientation of the tensile axis about 5° apart from the [001] – [$\bar{1}$11] symmetry line (see the insert in Fig. 1b). Such a choice of the chemical composition of the single crystal samples and their initial crystallographic orientation assured the B2 twin system to be activated during the crystal tensile deformation. Figure 1b shows stress-strain characteristics of the studied crystals together with tensile axis rotation in the insert. The sample was deformed until twins propagating in the form of L ü d e r s band filled its whole gauge length.

In order to verify the active twin system, the X-ray diffraction measurements were done on Bruker AXS Discover 8 diffractometer and the {111} pole figures were determined. Figure 2a presents {111} pole figure of a deformed single crystal. One can read the mutual positions of the matrix and twin lattices, which compared to the initial crystal lattice orientation verify the twin shear plane as the plane **B**, or crystallographically, the (111) plane. From three twin directions of <112> type laying on the **B** plane, the [$\bar{1}\bar{1}$2] is topologically forbidden (shear polarization condition) and the activation of [1$\bar{2}$1] direction is not plausible because of low orientation coefficient. Thus, it is reasonable to assume at this moment that the operating twin system is the B2 ≡ (111)[$\bar{2}$11].

The deformed crystal underwent further mechanical and chemical treatment aiming for preparation of specimen for transmission electron microscopy observations. Using spark erosion cutter the crystal was sliced into flat pieces parallel to the $A \equiv (\bar{1}11)$ plane (its choice as the cutting plane will be explained later on). The angles needed for proper cutting of the sample were calculated on the basis of the X-ray measurements (Fig. 2a). The trace of intersection of the A plane (dotted line) with the side surface of the sample was inclined 72° to the

tensile direction T, however the normal direction x_1 was deflected only about 2° from the plane. The correctness of the selection of the cutting angles was finally verified by the X-ray measurements (Fig. 2b). The next stage was thinning out the sample on the abrasive paper with higher and higher gradation. The final stage was electropolishing on the automatic STRUERS device using an etchant on the basis of the orthophosphoric acid. The electron microscopy investigations were carried out on JEOL 2010 ARP electron microscopy with acceleration voltage 200 kV.

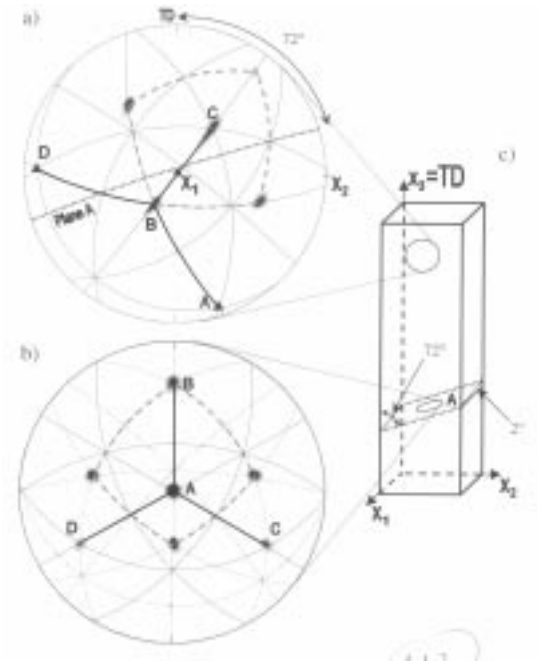

Fig. 2. {111} pole figure showing the appearance of twin lattice with the plane **B**≡(111) as the K1 habit plane of the twin transformation of a deformed single crystal (a); the orientation of the thin foils cut out from the twinned crystal parallel to the plane **A**≡ ($\bar{1}$11), which is the K_2 plane of the twin transformation (b); a scheme of the crystal sample from which the secondary sample was cut out. Note also the indicated places from which the pole figures were obtained (c)

On the other hand the table 1 presents $\boldsymbol{g}^{\circ}\boldsymbol{b}$ values for the cube a[100] and all possible classical Burgers vector dislocations and for diffraction vectors $\boldsymbol{g}$ = [020], $\boldsymbol{g}$ = [111], $\boldsymbol{g}$ = [002]. They were chosen in such a way so the sequence of visibility or vanishing of dislocation contrast: $\boldsymbol{g}$ = [020] – not visible, $\boldsymbol{g}$ = [111] – visible, $\boldsymbol{g}$ = [002] – not visible, was fulfilled only in the case of the Burgers vector a[100]. It is worth mentioning that **g** = [111] is common for both matrix and twin lattices, but the vectors $\boldsymbol{g}$ = [020], $\boldsymbol{g}$ = [002] are of the twin lattice only. The electron microscope used in the studies was equipped with a goniometric stage of two mutually perpendicular rotational axes of the inclination angles ±30°. The choice of the cutting plane of the foil as the ($\bar{1}$11) (plane $\boldsymbol{A}$) ensure availability of using all diffraction vectors shown in the table 1. The situation is presented graphically on the figure 3 which is a fragment of the stereographic projection on (001) plane. The length of the arrows indicate angular distances from the ($\bar{1}$11) pole to the respective planes (020), (111), (002), or alternatively, to the corresponding diffraction vectors.

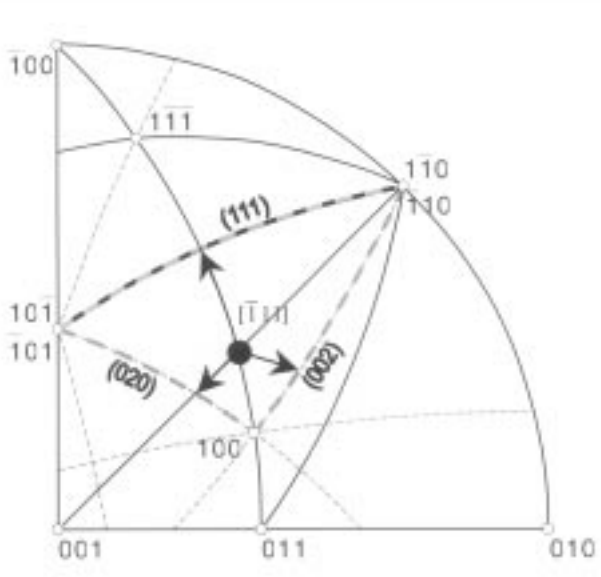

Fig. 3. Fragment of the stereographic projection of the B2 twin-matrix orientation relationship showing accessibility of diffraction vectors, **g** = [020], **g** = [111], and **g** = [002], applied in the experiment

TABLE 1
The $\boldsymbol{g}^{\circ}\boldsymbol{b}$ criterion of visibility (±1) or vanishing (0) of dislocation contrast of classical Burgers vector and cube dislocations

g / **b**	[111]	[020]	[002]
[100]	**1**	**0**	**0**
1/2[1$\bar{1}$0]	**0**	**–1**	**0**
1/2[10$\bar{1}$]	**0**	**0**	**–1**
1/2[011]	**1**	**1**	**1**
1/2[101]	**1**	**0**	**1**
1/2[110]	**1**	**1**	**0**
1/2[01$\bar{1}$]	**0**	**1**	**–1**

3. Results and discussion

The activation of mechanical twinning in the tensile Cu-8at.%Al single crystals is preceded by an appreciable incubation period of crystal deformation by slip. Depending on the initial orientation of the crystal it is possible to activate twin system belonging to either primary plane $\boldsymbol{B}$ or conjugate plane $\boldsymbol{C}$ [4]. The activation of the $C3$ twin system is already attained in the conditions of the first overshoot (Fig. 1a) while the

$B2$ twin system requires the conditions of the second overshoot to be achieved (Fig. 1b). In the paper [1] first experimental proves for the correct application of the correspondence matrix method through confirmation of the presence of cube dislocation inherited by the $C3$ twin were found. This paper widens the above studies on the case of $B2$ twinning associated with the second overshoot phenomenon. Comparison of the crystallography of both $C3$ and $B2$ twins is presented in the figure 4.

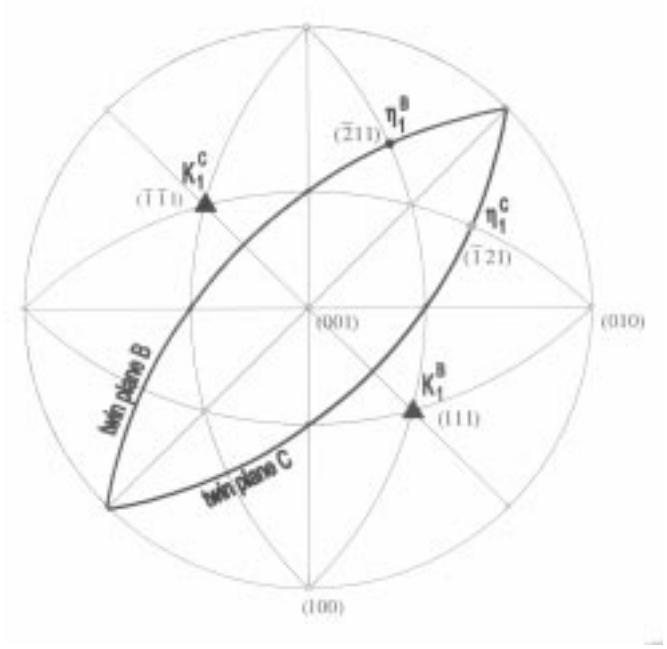

Fig. 4. The differences in crystallography of B2 and C3 twins generated in the tensile Cu-8at.%Al single crystals. The K_1 and η_1 symbols mean the twinning plane and the twinning direction respectively

On the other hand, equations 1-3 show successively the deformation S_{B2}, reindexation L_{B2} and correspondence C_{B2} matrices for the twin system identified at the end of the second overshoot tensile strains.

$$S_{B2} = \frac{1}{6}\begin{bmatrix} 4 & -2 & -2 \\ 1 & 7 & 1 \\ 1 & 1 & 7 \end{bmatrix} \tag{1}$$

$$L_{B2} = \frac{1}{3}\begin{bmatrix} -1 & 2 & 2 \\ 2 & -1 & 2 \\ 2 & 2 & -1 \end{bmatrix} \tag{2}$$

$$C_{B2} = \frac{1}{2}\begin{bmatrix} 0 & 1 & 1 \\ 1 & -1 & 1 \\ 1 & 1 & -1 \end{bmatrix} \tag{3}$$

$$v_T = Cv_M \tag{4}$$

$$n_T = n_M C^{-1} \tag{5}$$

Table 2 presents the crystallography of transformation of all slip planes and Burgers vectors of perfect dislocations, according to the transformation equations for any crystallographic direction (eq. 4) and plane (eq. 5), where the correspondence matrix C_{B2} is involved. As it is shown in the table 2, due to twin shear $a/2[011]$ Burgers vector dislocations belonging to the easy glide planes ***C*** and ***D*** turn into completely sessile configurations lying after the transformation on the cube planes and also having cube, $a[100]$, Burgers vector.

TABLE 2

Geometry of twin transformation of classical Burgers vector dislocations $a/2\langle 110\rangle\{111\}$ for twin system $B2 \equiv (111)\,[\bar{2}11]$ (G – glissile dislocation, S – sessile dislocation)

Matrix dislocation		Twin dislocation		Change of dislocation type
Burgers vector	Plane	Burgers vector	Plane	
a/2[0 1 $\bar{1}$]		a/2[0 $\bar{1}$ 1]		G→G
a/2[1 $\bar{1}$ 0]	B (1 1 1)	a/2[$\bar{1}$ 1 0]	(1 1 1)	G→G
a/2[1 0 $\bar{1}$]		a/2[$\bar{1}$ 0 1]		G→G
a/2[1 $\bar{1}$ 0]		a/2[$\bar{1}$ 1 0]		G→S
a/2[0 1 1]	C (1 1 $\bar{1}$)	a/2[1 0 0]	(0 0 2)	G→S
a/2[1 0 1]		a/2[1 1 0]		G→S
a/2[1 0 $\bar{1}$]		a/2[$\bar{1}$ 0 1]		G→S
a/2[0 1 1]	D (1 $\bar{1}$ 1)	a[1 0 0]	(0 2 0)	G→S
a/2[1 1 0]		a/2[1 0 1]		G→S
a/2[0 1 $\bar{1}$]		a/2[0 $\bar{1}$ 1]		G→G
a/2[1 0 1]	A ($\bar{1}$ 1 1)	a/2[1 1 0]	(1 $\bar{1}$1)	G→G
a/2[1 1 0]		a/2[1 0 1]		G→G

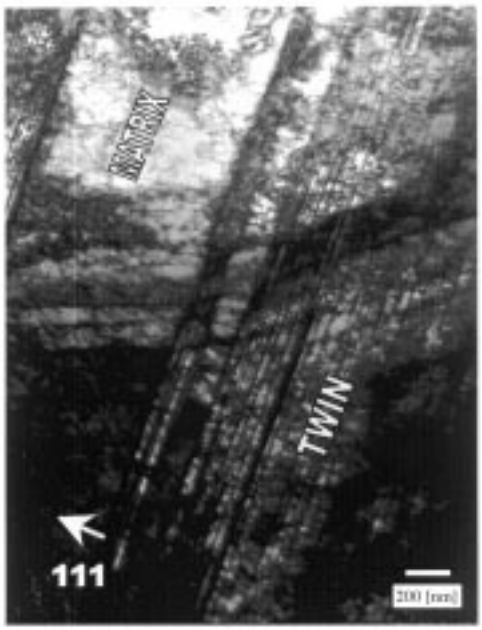

Fig. 5. Typical dislocation substructure of matrix-twin regions in the deformed Cu-8at.%Al single crystals

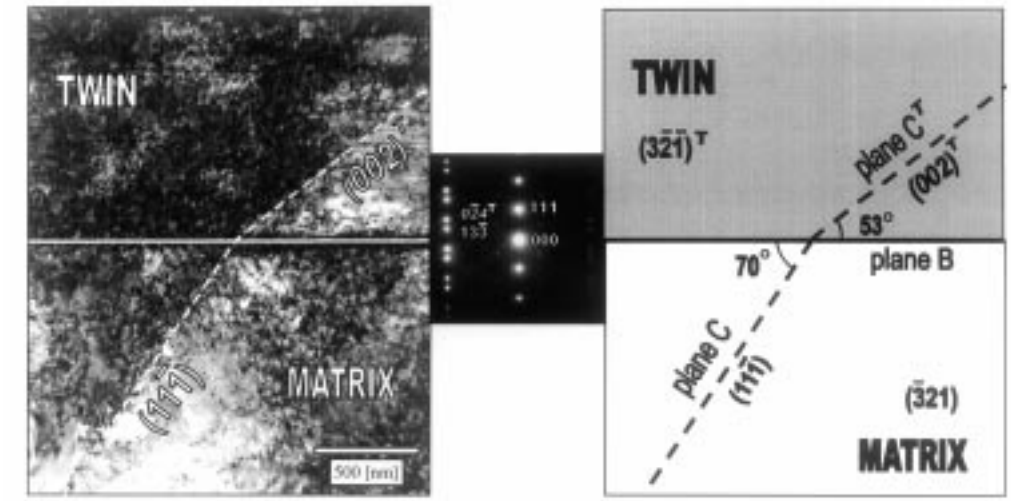

Fig. 6. Bright field multi-beam electron micrograph taken from the foil turned off to the edge-on position of the twin-matrix interface, where the plane of observation is parallel to the $(\bar{3}21)$ plane of the parent crystal, and the corresponding diffraction pattern with the scheme of geometry of a twin shear

The first stage of verification of the correctness of the correspondence matrix method was identification of the transformation of the slip plane $\boldsymbol{C} \equiv (11\bar{1})$ into the new configuration (002). Figure 5 shows the dislocation substructure of the Cu-8at.%Al single crystal deformed at the condition of the second overshoot. It is easy to distinguish between matrix and twin regions, where the latter is characterized by the regular dislocation arrangements parallel to the twinning plane $\boldsymbol{K_1}$. Figure 6 shows the dislocation substructure of the same region of the matrix-twin interface but at different perspective. The change of the inclination of the $\boldsymbol{C}$ plane trace (showed with the broken line) is clearly visible during the passage from the matrix into the twin. The identification of the plane transformed by the twin shear was conducted using the trace analysis method on the stereographic projection. Figure 7 illustrates the stereographic projection of the matrix crystal standardized on the (001) plane (a) and the corresponding $B2$ twin lattice (b). The dotted line is the trace of the $(\bar{3}21)$ plane which is parallel to the plane of observation. The angles between directions of intersection of plane $\boldsymbol{B}$ (heavy line) and planes $\boldsymbol{A}$, $\boldsymbol{C}$, $\boldsymbol{D}$ (dotted line) with the plane of observation were also measured. Similar procedure was applied for the twin lattice, and the analyzed planes were $\boldsymbol{B}$, $\boldsymbol{A^T}$ $(1\bar{1}\bar{1})$, $\boldsymbol{C^T}$ (002), $\boldsymbol{D^T}$ (020). The angles between the traces of **B** plane and the planes $\boldsymbol{C}$ and $\boldsymbol{C^T}$ were 70° and 53° respectively. They prove that the twin transformation of the $\boldsymbol{C}$ plane follows exactly the predictions of the correspondence matrix method. It is then expected that dislocation laying on the planes $\boldsymbol{C} \equiv (11\bar{1})$ and $\boldsymbol{D} \equiv (1\bar{1}1)$ will turn into the sessile configurations on the planes $\boldsymbol{C^T} \equiv (002)$, $\boldsymbol{D^T} \equiv (020)$ increasing thus the "strengthening" of dislocation substructure and hence the resistance to the plastic deformation of the twin region.

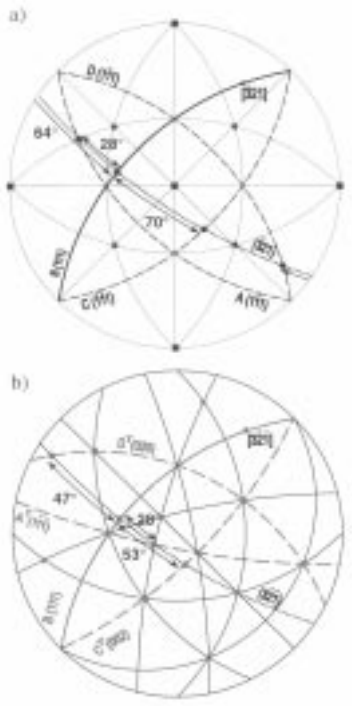

Fig. 7. Stereographic projection of a matrix crystal standardized on the (001) plane (a) and the corresponding B2 twin lattice (b). The dotted line is the trace of the $(\bar{3}21)$ plane which is parallel to the plane of observation. The pair numbers shown on the two corresponding projections in the figure: (28°,28°), (70°, 53°), (64°,47°) indicate the

angles of the traces of the planes ***A, C*** and ***D*** with the twin interface line respectively

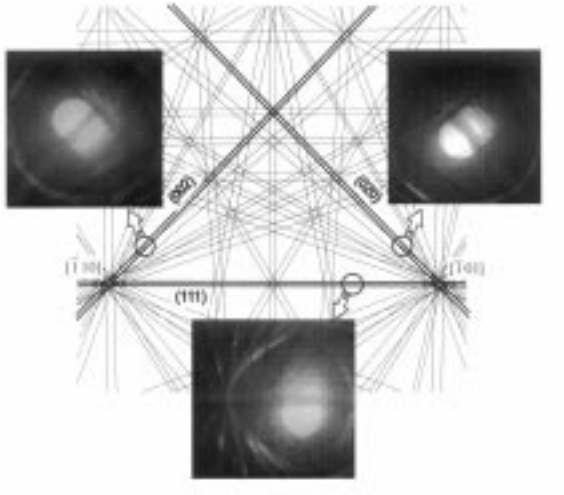

Fig. 8. Kikuchi line patterns with marked points showing the diffraction conditions at which the morphological images of figures 9 and 13 were taken

The second stage of verification of the correctness of the correspondence matrix method was identification of the transformation of the $a/2[011]$ Burgers vector dislocation into the cube configuration of $a[100]$(see the table 2). Figure 8 shows the common for both matrix and twin lattice K i k u c h i lines pattern on the plane corresponding with the cutting plane of the thin foil. The locations of the sample position at which the morphological pictures were taken are marked in the figure. As it was already mentioned the choice of the diffraction vectors $\boldsymbol{g} = [020]$ and $\boldsymbol{g} = [002]$ was critical for the unambiguous identification of the cube dislocation (see the table 1). Figure 9 show the dislocation substructure of the twin seen in the operating reflections $\boldsymbol{g} = [020]$ and $\boldsymbol{g} = [111]$ and $\boldsymbol{g} = [002]$ respectively. The twin regions contain clearly visible stacking faults perpendicular to the $\boldsymbol{K_1}$ plane. The more the $\boldsymbol{K_1}$ plane is inclined to the

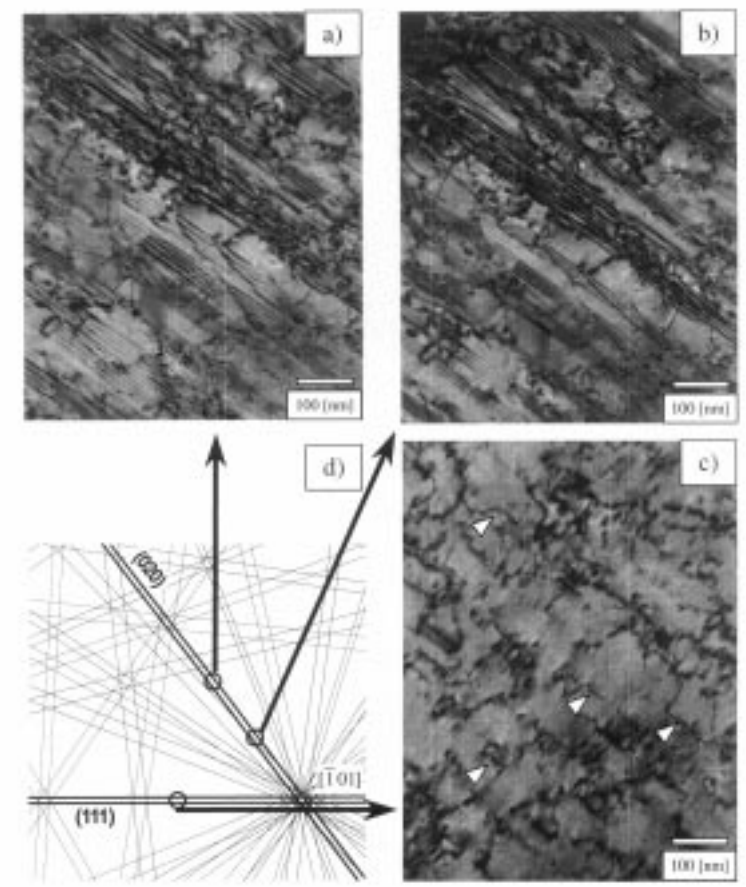

Fig. 9. Two-beam bright field micrographs taken at different diffraction conditions, $\boldsymbol{g} = [020]$ (a), $\boldsymbol{g} = [111]$ (b) and $\boldsymbol{g} = [002]$ (c) marked schematically in (d). Note also the extrinsic stacking faults associated with Frank dislocations well seen in (a) and (c) and totally vanished in (b) where the plane of the faults takes the edge-on position

incident beam the effect of larger screening of dislocation contrast by the stacking faults is observed. In order to minimize this effect, the pictures in the diffraction conditions $\boldsymbol{g}$ = [020] and $\boldsymbol{g}$ = [002] were taken in the

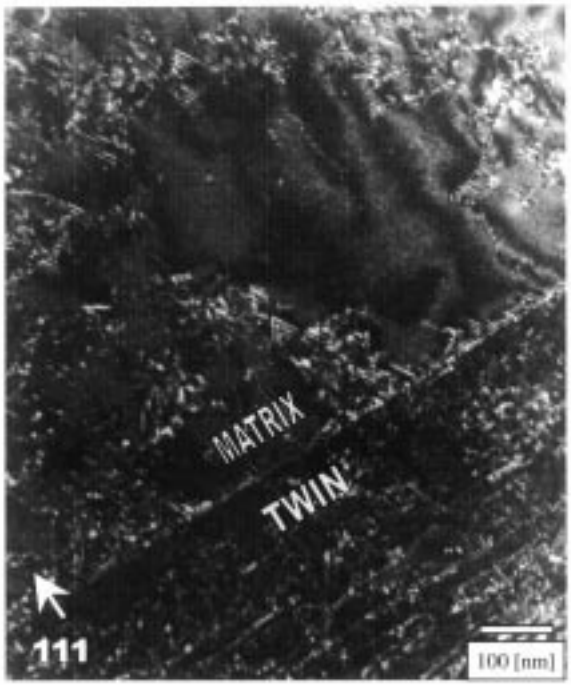

Fig. 10. Weak-beam electron micrograph of the typical dislocation substructure of the B2 twin-matrix crystal region showing again regularly distributed dislocation arrangements inside the twin

positions as close as possible to the symmetry axes $(\bar{1}10)$ and $(\bar{1}01)$, but also taking into consideration the necessity of getting proper two-beam conditions of dislocation image formation. The stacking faults are invisible at the diffraction vector $\boldsymbol{g}$ = [111], because at this position the plane of stacking faults is parallel to the incident electron beam.

It is worth to emphasize again that the structure of the matrix is morphologically distinctly different from the structure of the twin (Fig. 10). On the matrix side there can be some dislocations tangles observed, however inside the twin the dislocation substructure is ordered, cut by the regular arrangements parallel to the habit plane. They were identified in the paper [1] as the partial Frank dislocations associated with the extrinsic stacking faults that are visible at the operating diffraction vectors $\boldsymbol{g}$ = [020] (Fig. 9a) and $\boldsymbol{g}$ = [002] (Fig. 9b). Some examples of the identified extrinsic Frank dislocations are marked by white arrows in the figure 9c. It is very important to emphasize that the dislocation substructure contain big amount of characteristic dislocations' segments that can be residue after an operation of active pole sources (examples are marked with arrows in the figure 11a). They consist of dislocation $\boldsymbol{b_T}$ laying on the $\boldsymbol{K_1}$ plane and to arms forming pole dislocations sheared to the twin lattice (Fig. 12). The dislocation $\boldsymbol{b_T}$ can dissociate according to the reaction in the figure 12. In result, a Frank dislocation $*\boldsymbol{b_T}$ and two Shockley dislocations $\boldsymbol{T}$ are formed that while propagating will spread the external stacking fault out inside the twin (Fig. 12b). The remaining arrangement consisting of Frank dislocation and two arms of the pole dislocation form a very stable and sessile configurations. Finally, the figure 13

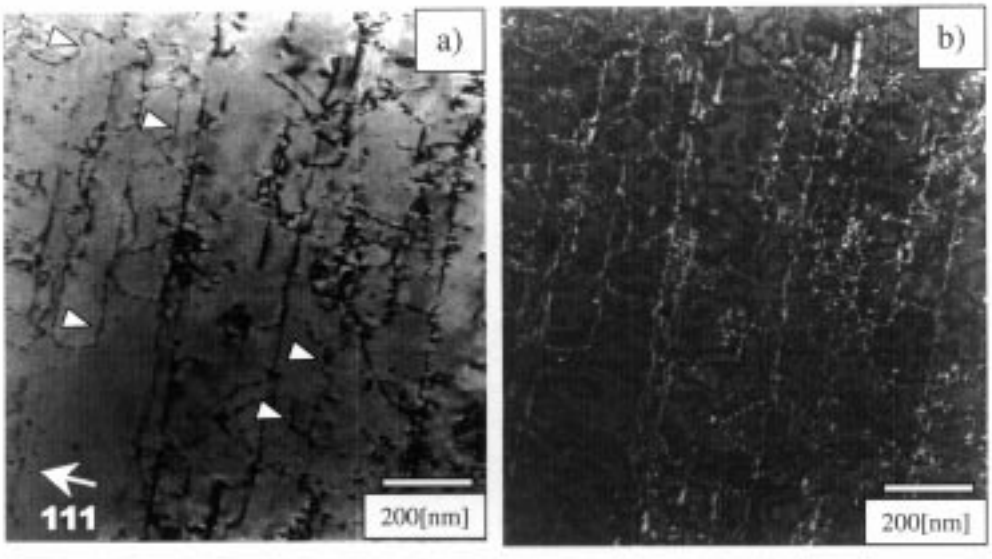

Fig. 11. Two-beam bright field micrograph of the dislocations of the B2 twin (a) and the corresponding image taken by weak-beam technique (b). Note many zigzag-like dislocation configurations (marked by white arrows) left in the deformed crystal after possible operation of the dislocation pole mechanism

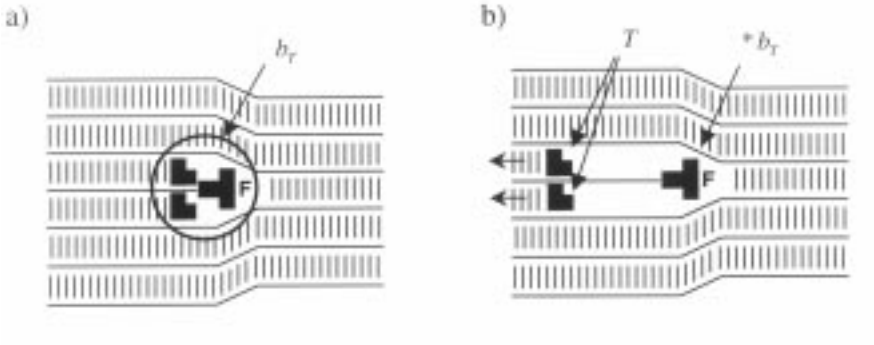

Fig. 12. A scheme showing geometry of dislocation triplet equivalent to the cube dislocation (a) and its natural dissociation process according to the reaction $b_T = *b_T + T + T$ (b), which explains the formation of extrinsic Frank dislocation network

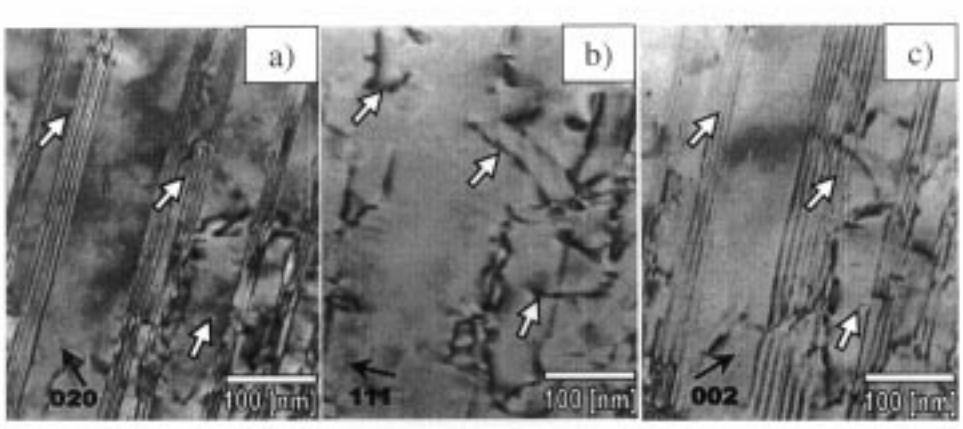

Fig. 13. The enlarged fragment of the dislocation image from figure 9. Note the [100] Burgers vector dislocations (marked by white arrows) well seen in (b) and totally vanished in (a) and (c). Note also the extrinsic stacking faults associated with Frank dislocations well seen in (a) and (c) and totally vanished in (b) where the plane of the faults takes the edge-on position

illustrates the identification of the cube dislocation. One can clearly see that segments of the a[100] dislocation (marked with the white arrows) are visible only at the $\boldsymbol{g}$ = [111] diffraction condition (see table 1) so, the difference in the amount and configuration of the defects between matrix and twin is of great importance. The twin regions are filled with the ordered arrangements of a dense three-dimensional network of the sessile dislocations, whereas the matrix region is not. The presence of the fully sessile cube/Frank dislocation arrangements strongly indicates the transformational reasons for the rapid increase of the twin hardening as it was reported in [1].

4. Summary

The paper adds to the contemporary literature another experimental proves for the existence of the cube dislocations formed during mechanical twinning of FCC single crystals. The obtained results confirm the fact that the correspondence matrix approach is the universal method for the predictions of twin transformation of dislocations. It allows to model processes of the structure change everywhere where the homogeneous shear of the material containing defects of the crystal lattice takes place. It is plausible that the scope of the application of the method can be successfully widen on e.g. martensitic transformations associated with the simple shear crystal deformation, for example FCC→HCP in cobalt [13]. Therefore, it is to emphasize that the presented here analysis can be also used to prepare suitable structure observations of the materials that underwent such martensitic transformations.

Acknowledgements

The financial support of the State Committee for Scientific Research of Poland under the grant number 3T08A 080 29 and AGH University of Science and Technology, Cracow, Poland under the grant numbers 11.11.180.255 and 10.10.180.281 is acknowledged.

REFERENCES

[1] Z.S. Basinski, M.S. Szczerba, M. Niewczas, J.D. Embury, S.J. Basinski, La Revue de Métallurgy-CIT/Science et Génie des Matériaux **94**, 1037 (1997).

[2] J.W. Christian, S. Mahajan, Progress in Materials Science **39**, 1 (1995).

[3] Z.S. Basinski, M.S. Szczerba, J.D. Embury, Philosophical Magazine A **76**, 743 (1997).

[4] M.S. Szczerba, T. Bajor, T. Tokarski, Philosophical Magazine **84**, 481 (2004).

[5] A.W. Sleeswyk, C.A. Verbraak, Acta Metallurgica **9**, 917 (1961).

[6] N. Jia, Y.D. Wang, S.D. Wu, W.Z. Han, Y.N. Wang, J.N. Deng, P.K. Liaw, Scripta Materialia **54**, 1247 (2006).

[7] A.A. Salem, S.R. Kalidindi, R.D. Doherty, Acta Materialia **51**, 4225 (2003).

[8] G.R. Purdy, Scripta Materialia **47**, 181 (2002).

[9] M.R. Barnett, C.H.J. Davies, X. Ma, Scripta Materialia **52**, 627 (2005).

[10] M.R. Barnett, Z. Keshavarz, A.G. Beer, D. Atwell, Acta Materialia **52**, 5093 (2004).

[11] G. Garces, M. Rodriguez, P. Perez, P. Adeva, Materials Science and Engineering A **419**, 357 (2006).

[12] Y. Chiu, F. Grégori, H. Inui, P. Veyssière, Philosophical Magazine **84**, 3235 (2004).

[13] B.A. Bilby, Philosophical Magazine **44**, 782 (1953).

Received: 10 March 2007.